Distributed MIMO Underwater Systems: Receiver Design and Software-defined Testbed Implementation

George Sklivanitis, Yi Cao, Stella N. Batalama, Weifeng Su
Department of Electrical Engineering, The State University of New York at Buffalo, Buffalo, NY 14260-2050
Email: {gsklivan, yicao, batalama, weifeng}@buffalo.edu

***Abstract*—We design, implement, and evaluate an acoustic receiver structure for distributed multi-input and multi-output (MIMO) underwater systems that accounts for multiple carrier frequency offsets (CFOs) and multiple timing offsets (TOs) encountered in real deployments of underwater communication systems. We focus on challenging practical issues that arise in underwater acoustic sensor network setups where co-located multi-antenna sensor deployment is not feasible due to power, computation, and hardware limitations. In this paper, we utilize distributed underwater sensors to form virtual MIMO underwater systems without requiring frequency or time synchronization. The proposed receiver consists of a bank of matched filters (one per effective CFO) at each receive antenna, followed by an information symbol detector. Each filter in the bank is sampled at the symbol rate with sampling timing selected according to the corresponding TO. We evaluate in real-time the performance of our algorithmic developments in a software-defined underwater testbed that utilizes in-house built software-defined acoustic modems (SDAMs). Experimental studies in both indoor, lab-controlled (tank) and outdoor (lake) real-world environments demonstrate superior bit-error-rate (BER) receiver performance compared to receiver designs that are not able to accommodate multiple CFOs and multiple TOs.**

***Index Terms*—Underwater, distributed antennas, MIMO, carrier frequency offset, time offset, software-defined radio, testbed**

I. Introduction

Underwater acoustic (UWA) communications is an emerging research area with a wide range of commercial and military applications such as pollution monitoring, surveillance, search, and rescue operations, oil exploration, to name a few. A key challenge in the design of UWA communication links stems from the characteristics of the UWA channel which exhibits high path loss, extended multipath delay spread, high and variable propagation delay, and large Doppler spread [1].

Recently, multi-input and multi-output (MIMO) techniques have attracted considerable attention in order to increase UWA channel capacity without penalizing precious power and bandwidth resources [2]. However the deployment of co-located MIMO transceivers in realistic underwater acoustic network (UAN) setups can be practically challenging due to power, computation, and hardware constraints. In this work we exploit spatial diversity by forming virtual (distributed) MIMO antenna systems in distributed antenna setups. In this setup, cooperation between geographically separated antenna transceivers of the virtual MIMO cluster is required in order to achieve both carrier frequency and timing synchronization.

Cooperative synchronization algorithms for distributed transceivers with multiple carrier frequency offsets (CFOs) and timing offsets (TOs) due to independent clock oscillator circuits have been investigated for terrestrial communications [3], [4], [5]. However, most existing distributed MIMO receiver designs exploit only the effect of CFO to the phase of the received signal and do not consider its severe effect to the symbol energy attenuation at the receiver output. Indeed, it is evident that, even in single-input and single-output (SISO) systems [6], the output of the pulse matched filter experiences amplitude degradation due to lack of carrier frequency synchronization. Thus, in distributed MIMO systems, it is expected that multiple CFOs will have different symbol-energy attenuation effects at the receiver output which should be addressed properly. In addition, existing work in distributed MIMO literature assume perfectly time-synchronous transmission and reception, which is not compatible with the very nature of distributed antenna systems. On the contrary, existing work in cooperative MIMO UWA communications considers the problem of multiple CFOs due to different Doppler-distorted propagation paths between spatially separated mobile transceivers [7] and proposes a decision feedback equalizer at the receiver. The work in [8] assumes transceiver coordination and studies iterative receiver designs for quasi-synchronous distributed underwater systems.

In this paper, motivated by our work in [9], we propose a receiver structure for distributed MIMO UWA communication systems that accounts for multiple CFOs and multiple TOs due to differences in distributed local oscillators and propagation delays, respectively. Contrary to prior-art in distributed MIMO systems, the proposed receiver accounts for the effect of multiple CFOs and multiple TOs on symbol energy. The proposed receiver structure uses a matched filter (MF) bank front-end (one MF per effective CFO) at each receive antenna and samples the output of each matched filter at the symbol rate with sampling timing determined by the corresponding TO. The MF bank is followed by the maximum likelihood (ML) detector that is derived for the given receiver front-end. Real-time experimental validation of the receiver is performed with in-house built software-defined underwater acoustic modems (SDAMs) [10], [11], [12] in indoor, lab-controlled (tank) and outdoor (lake) underwater environments. The capability of the proposed receiver to accommodate successfully multiple CFOs and multiple TOs is demonstrated by bit-error-rate (BER)

performance results evaluated on software-defined testbeds in real-time during real-world experiments.

The rest of the paper is organized as follows. In Section II, we review the system model of the distributed MIMO UWA system, where distributed transmit and receive antennas introduce multiple CFOs and multiple TOs. Section III presents the proposed receiver structure, while Section IV describes the configuration details of the software-defined testbed implementation. Experimental results and proposed receiver performance in both indoor (tank) and outdoor (lake) deployments are illustrated and discussed in Section IV. Finally, conclusions are drawn in Section V.

II. System Model

We consider a single-carrier narrowband underwater communication system with M_t distributed transmit antennas and M_r receive antennas (Fig. 1). Both transmit and receive antennas are geographically separated and cannot utilize a common oscillator to generate carrier signals. The bandpass signal sent from the i-th transmit antenna can be written as

$$x_i(t) = \sum_{n=1}^{N} Re\left\{ s_i^{(n)} g(t - nT_s) e^{j2\pi(f_c+\mu_i)t} \right\} \quad (1)$$

where N is the symbol-record size, $s_i^{(n)}$ is the information symbol sent by the i-th transmit antenna at the n-th time slot, $g(t)$ is the pulse shaping signal, T_s is the symbol duration, f_c is the assumed target carrier frequency ($f_c >> B$), B is the selected signal bandwidth, and μ_i denotes the carrier frequency drift of the i-th transmit antenna.

We assume that all signals propagate over independent time-varying multipath fading underwater acoustic channels with impulse response of the following general form

$$c(\tau, t) = \sum_{m=1}^{M} h^m(t)\delta(\tau - \tau^m(t)) \quad (2)$$

where M denotes the total number of paths (assumed to be the same for all signals), $h^m(t)$ is the m-th path's amplitude coefficient, and $\tau^m(t)$ is the time-varying path delay. In our studies we consider that the channel amplitude and delay parameters change slowly and are time invariant during N symbol transmission periods [13]. Furthermore, for the purposes of this paper we consider non mobile, static underwater setups, therefore Doppler scaling is considered negligible. We note that the proposed receiver can be easily extended to account for mobility.

As a result at the receiver side (Fig. 1), the lowpass equivalent signal at the j-th receive antenna, $j = 1, 2, \ldots, M_r$ can be written as

$$r_j(t) = \frac{1}{2} \sum_{i=1}^{M_t} \sum_{m=1}^{M} \tilde{h}_{i,j}^m e^{j2\pi\Delta f_{i,j} t} x_i(t - \tau_{i,j}^m) + n_j(t) \quad (3)$$

where $\tilde{h}_{i,j}^m \triangleq h_{i,j}^m e^{-j2\pi(f_c+\mu_i)\tau_{i,j}^m}$, $h_{i,j}^m$ represents the m-th path channel coefficient from the i-th transmit antenna to the j-th receive antenna, $\tau_{i,j}^m$ denotes the m-th path propagation delay from the i-th transmit antenna to the j-th receive antenna, $\Delta f_{i,j} = (f_c + \mu_i) - (f_c + \nu_j) = \mu_i - \nu_j$ denotes the carrier frequency offset between the i-th transmit antenna and the j-th receive antenna (ν_j denotes the carrier frequency drift at the j-th receive antenna), and $n_j(t)$ is the lowpass noise at the j-th receiver with bandwidth B and power spectral density N_0.

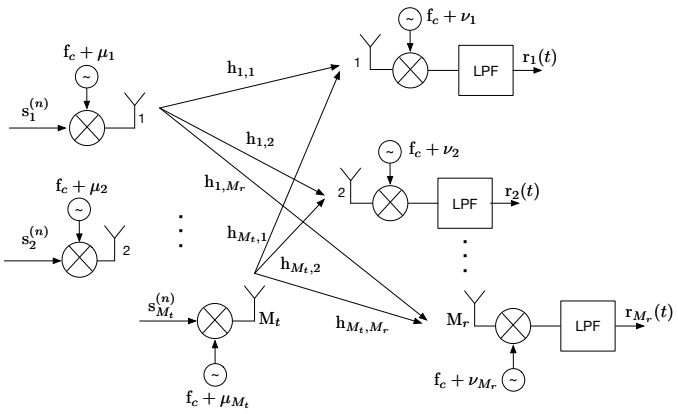

Fig. 1. Distributed MIMO UWA setup with spatially separated M_t transmit and M_r receive antennas.

We consider narrowband underwater systems that operate at high acoustic frequencies (i.e. $90 - 100$ kHz) with symbol duration T_s greater than the multipath spread of the channel, therefore the narrowband assumption ($f_c >> B$) is justified and the channel-path transfer functions are flat over the entire bandwidth B [14]. As multiple paths M are not resolvable and intersymbol interference terms are arguably negligible we can rewrite the received signal at the j-th receive antenna, $j = 1, 2, \ldots, M_r$ as follows

$$r_j(t) = \frac{1}{2} \sum_{i=1}^{M_t} \sum_{n=1}^{N} \tilde{h}_{i,j} e^{j2\pi\Delta f_{i,j} t} s_i^{(n)} g(t - nT_s - \tau_{i,j}) + n_j(t) \quad (4)$$

where $\tilde{h}_{i,j} \triangleq h_{i,j} e^{-j2\pi(f_c+\mu_i)\tau_{i,j}}$, $h_{i,j}$ represents the complex channel coefficient, and $\tau_{i,j}$ denotes the propagation delay from the i-th transmit antenna to the j-th receive antenna. The received signal model in (4) considers a single dominant propagation path together with weak multipath components.

III. Receiver Design

The receiver front-end design for the j-th receiving element is depicted in Fig. 2. The proposed receiver first proceeds with estimation of the unknown CFOs ($\Delta f_{1,j}, \Delta f_{2,j}, \ldots, \Delta f_{M_t,j}$) and TOs ($\tau_{1,j}, \tau_{2,j}, \ldots, \tau_{M_t,j}$) between the j-th receive antenna element and i-th transmit antenna, $i = 1, 2, \ldots, M_t$. As CFO and TO estimation is out of the scope of this paper we will briefly describe the estimation process during the software-defined testbed setup in Section IV.

Motivated by our work in [9] the receiver consists of M_t parallel matched filters at each receive antenna. The matched filters operate on the lowpass filtered received signals, and each of the filters targets a specific link CFO, $\Delta f_{i,j}$. The filter outputs are then sampled at the symbol rate with sampling timing that is determined by the estimated link TO, $\tau_{i,j}$. More specifically, at the j-th receive antenna, $j = 1, 2, \ldots, M_r$, the matched filter on the m-th, $m = 1, 2, \ldots, M_t$, branch

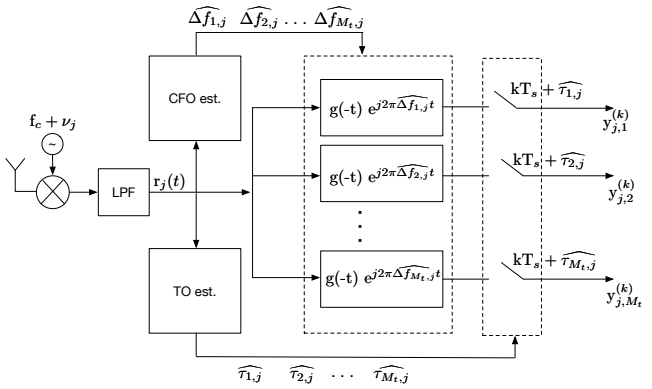

Fig. 2. Receiver front-end design of the j-th receiving element affected by multiple CFOs and multiple TOs.

is adjusted to $g(-t)e^{j2\pi\widehat{\Delta f_{m,j}}t}$ to accommodate CFO $\Delta f_{m,j}$. The filter output is then sampled at $t = kT_s + \hat{\tau}_{m,j}$ to accommodate TO $\tau_{m,j}$. As a result, the sampled output of the matched filter at the m-th branch at the k-th time slot can be written as in [9]

$$y^{(k)}_{j,m} = \boldsymbol{\psi}^{(k)}_{j,m}\left[\boldsymbol{s}^{(k-1)^T}\boldsymbol{s}^{k^T}\boldsymbol{s}^{(k+1)^T}\right]^T + N^{(k)}_{j,m} \tag{5}$$

where $\boldsymbol{\psi}^{(k)}_{j,m}$ denotes the vector of the coefficients of symbols from the $(k-1)$-th, k-th and $(k+1)$-th time slots with size $3M_t$. Vector $\boldsymbol{\psi}^{(k)}_{j,m}$ is given by

$$\boldsymbol{\psi}^{(k)}_{j,m} \triangleq \frac{1}{2}\begin{bmatrix} \tilde{h}_{1,j}e^{j2\pi\Delta f_{1,j}(kT_s+\tau_{m,j})}G_{1,j,m,1} \\ \vdots \\ \tilde{h}_{M_t,j}e^{j2\pi\Delta f_{M_t,j}(kT_s+\tau_{m,j})}G_{M_t,j,m,1} \\ \tilde{h}_{1,j}e^{j2\pi\Delta f_{1,j}(kT_s+\tau_{m,j})}G_{1,j,m,0} \\ \vdots \\ \tilde{h}_{M_t,j}e^{j2\pi\Delta f_{M_t,j}(kT_s+\tau_{m,j})}G_{M_t,j,m,0} \\ \tilde{h}_{1,j}e^{j2\pi\Delta f_{1,j}(kT_s+\tau_{m,j})}G_{1,j,m,-1} \\ \vdots \\ \tilde{h}_{M_t,j}e^{j2\pi\Delta f_{M_t,j}(kT_s+\tau_{m,j})}G_{M_t,j,m,-1} \end{bmatrix}^T, \tag{6}$$

where

$$G_{i,j,m,p} \triangleq \int_{-\infty}^{+\infty} g(pT_s + \hat{\tau}_{m,j} - \tau_{i,j})g(-\tau)e^{j2\pi(\widehat{\Delta f_{m,j}} - \Delta f_{i,j})\tau}\, d\tau,$$

$\boldsymbol{s}^{(k)} = \left[s^{(k)}_1, \cdots, s^{(k)}_{M_t}\right]^T$ is the symbol vector sent at the k-th time slot from M_t distributed transmit antennas and $N^{(k)}_{j,m} = \{n_j(t)\} * \left\{g(-t)e^{j2\pi\widehat{\Delta f_{m,j}}t}\right\}|_{t=kT_s+\hat{\tau}_{m,j}}$ is the sampled noise at the matched filter output of the m-th branch, at the j-th receive antenna.

Sampled filter outputs $y^{(k)}_{j,m}$, $m = 1, \ldots, M_t$ are then collected from all M_t branches at the j-th receive antenna and form the received signal vector of size M_t as

$$\boldsymbol{Y}^{(k)}_j = \left[y^{(k)}_{j,1}, \cdots, y^{(k)}_{j,M_t}\right]^T = \boldsymbol{\psi}^{(k)}_j \boldsymbol{S}^T + \boldsymbol{N}^{(k)}_j \tag{7}$$

where $\boldsymbol{\psi}^{(k)}_j = \left[\boldsymbol{\psi}^{(k)^T}_{j,1} \cdots \boldsymbol{\psi}^{(k)^T}_{j,M_t}\right]^T$ is the coefficient matrix at the j-th receiving element, $\boldsymbol{S} = \left[\boldsymbol{s}^{(k-1)^T}\boldsymbol{s}^{(k)^T}\boldsymbol{s}^{(k+1)^T}\right]$, and $\boldsymbol{N}^{(k)}_j = \left[N^{(k)}_{j,1}, \cdots, N^{(k)}_{j,M_t}\right]^T$ is the vector of sampled noise at the j-th receive antenna. Finally, we stack $\boldsymbol{Y}^{(k)}_j$, $j = 1, \ldots, M_r$, from all M_r distributed receive antennas in a received signal vector of size M_tM_r, which is denoted as

$$\boldsymbol{Y}^{(k)} = \left[\boldsymbol{Y}^{(k)^T}_1 \cdots \boldsymbol{Y}^{(k)^T}_{M_r}\right]^T = \boldsymbol{\Psi}^{(k)}\boldsymbol{S}^T + \boldsymbol{N}^{(k)} \tag{8}$$

where $\boldsymbol{\Psi}^{(k)} = \left[\boldsymbol{\psi}^{(k)^T}_1 \cdots \boldsymbol{\psi}^{(k)^T}_{M_r}\right]^T$ is the corresponding coefficient matrix, and $\boldsymbol{N}^{(k)} = \left[\boldsymbol{N}^{(k)^T}_1 \cdots \boldsymbol{N}^{(k)^T}_{M_r}\right]^T$ is the corresponding sampled noise vector.

Transmitted symbols $\boldsymbol{s}^{(k)}$ sent at the k-th time slot from M_t distributed transmit antennas are then detected using the optimal ML detector for this given receiver front-end structure. The ML detector is given by

$$\widehat{\boldsymbol{s}^{(k)}} = \underset{\boldsymbol{s}^{(k-1)},\boldsymbol{s}^{(k)},\boldsymbol{s}^{(k+1)}}{\arg\max}\ P(\boldsymbol{Y}^{(k)}) \tag{9}$$

where $P(\boldsymbol{Y}^{(k)})$ is the probability density function of $\boldsymbol{Y}^{(k)}$ which is

$$P(\boldsymbol{Y}^{(k)}) = \frac{1}{(2\pi)^{\frac{M_tM_r}{2}}|\Sigma|^{\frac{1}{2}}} exp\Bigg\{-\frac{1}{2}\left(\boldsymbol{Y}^{(k)} - \boldsymbol{\Psi}^{(k)}\boldsymbol{S}^T\right)^H \Sigma^{-1} \times \left(\boldsymbol{Y}^{(k)} - \boldsymbol{\Psi}^{(k)}\boldsymbol{S}^T\right)\Bigg\}. \tag{10}$$

In (10), we denote by Σ the covariance matrix of the overall noise vector $\boldsymbol{N}^{(k)}$ of size $M_tM_r \times M_tM_r$ which is given by

$$\Sigma = \begin{pmatrix} Var(N^{(k)}_{1,1}) & Cov(N^{(k)}_{1,1},N^{(k)}_{1,2}) & \cdots & Cov(N^{(k)}_{1,1},N^{(k)}_{M_r,M_t}) \\ Cov(N^{(k)}_{1,2},N^{(k)}_{1,1}) & Var(N^{(k)}_{1,2}) & \cdots & Cov(N^{(k)}_{1,2},N^{(k)}_{M_r,M_t}) \\ \vdots & \vdots & \ddots & \vdots \\ Cov(N^{(k)}_{M_r,M_t},N^{(k)}_{1,1}) & Cov(N^{(k)}_{M_r,M_t},N^{(k)}_{1,2}) & \cdots & Var(N^{(k)}_{M_r,M_t}) \end{pmatrix}$$

where $Var(N^{(k)}_{i,j})$ and $Cov(N^{(k)}_{i,j}, N^{(k)}_{i',j'})$ are the variance of $N^{(k)}_{i,j}$ and covariance between $N^{(k)}_{i,j}$ and $N^{(k)}_{i',j'}$, respectively.

IV. Software-defined Testbed Setup

The capability of the proposed receiver to accommodate multiple CFOs and multiple TOs is practically demonstrated in an indoor, lab-controlled tank environment, and an outdoor (Lake Erie) environment, using software-defined testbed setups. The proposed receiver front-end is implemented in software-defined acoustic modems (SDAMs) that are built in-house. Both software-defined underwater acoustic testbeds consider $M_t = 2$ distributed transmit, and $M_r = 1$ receive antennas.

Fig. 3 depicts the equipment setup for two transmit SDAMs (center) which are controlled through a Gigabit Ethernet switch by a single host-PC. Both SDAMs are based on the USRP N210 platform and are equipped with LFTX daughtercards that operate from DC to 30 MHz. LFTX daughtercards are connected to linear wideband power amplifiers (PA), BenthowareBII − 5002, which provide maximum output power of 192 dB and can support up to 300 kHz bandwidth. Subsequently, SDAMs are interfaced with Teledyne RESON TC4013 acoustic transducers, which are deployed in the water.

Fig. 3 also illustrates the equipment setup at the receiver side (right). The received signal is first bandpass filtered by a voltage preamplifier (PreAmp), Teledyne VP2000, and then downconverted to baseband by the circuitry of the LFRX

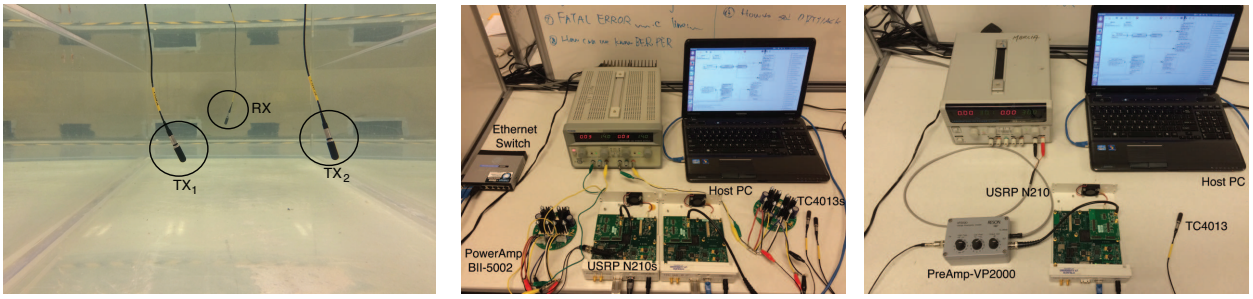

Fig. 3. Water tank testbed setup: Two software-defined acoustic transmit and one receive modems (from left to right) are interfaced with $M_t = 2$ and $M_r = 1$ acoustic transducers, respectively.

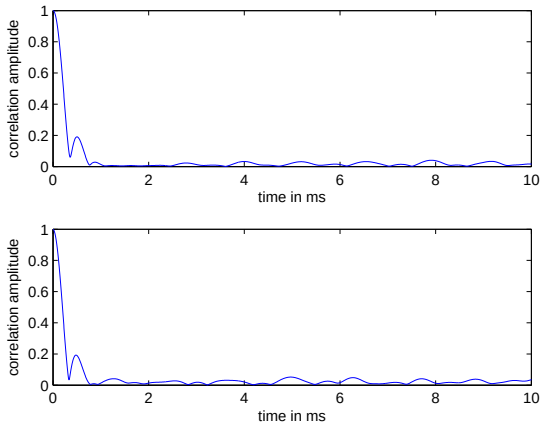

Fig. 4. Normalized channel response in water tank.

daughtercard. The voltage preamplifier at the receive SDAM is able to compress noise outside of the desired frequency band with user configurable bandpass filters and provides adjustable gain selection from 0 to 50 dB. The receive modem is also interfaced with Teledyne's TC4013 acoustic transducer.

Baseband processing for both transmit and receive SDAMs takes place at the host-PC. Particularly, we use GNU Radio, an open-source software framework for the implementation of the transmitters, and Universal Hardware Driver (UHD) for communicating the generated baseband samples to the SDAM. Custom baseband signal processing blocks that implement the proposed receiver were implemented in GNU Radio.

In both tank and Lake Erie experiments we consider packet transmissions of binary phase-shift keying (BPSK) modulated bits that are shaped with square-root-raised-cosine (SRRC) pulses of duration $T_s = 1.3107$ ms, and use roll-of factor $\alpha = 0.35$. Modulated symbols are then interpolated with 256 samples per symbol before converted to analog waveforms by the digital-to-analog (DAC) converter of the USRP-based SDAMs. Packet size is set to $N = 64$ information bits for both distributed transmitters TX_1 and TX_2, while timing recovery and channel estimation at the receiver is achieved by using a maximum length PN-sequence (m-sequence) of length 127 at the packet preamble. Maximum length sequences have good periodic correlation properties and are suitable for channel estimation and synchronization. Particularly, each transmitter is assigned to orthogonal m-sequences to enable estimation of multiple TOs. On the other hand, CFOs per effective link (e.g. TX_1-RX) are calculated by peak-picking the periodogram of the transmitted data of TX_1 during silent periods of TX_2. Experiments are conducted for different settings of TOs and CFOs, which are user configurable parameters available in the GNU Radio implementation of transmitters TX_1 and TX_2.

A. Tank Tests

In the experiments performed in a water tank of size $8\,\mathrm{ft} \times 2.5\,\mathrm{ft} \times 2\,\mathrm{ft}$, both transmitters use the same transmission power and carrier frequency $f_c = 100$ kHz, and are positioned 16 inches apart from the receiver RX, while the distance between TX_1 and TX_2 is set to 7 inches. The proposed testbed setup mitigates strong multipath reflections due to the small size of the tank. Fig. 4 depicts the normalized channel response for our water tank experiments, which confirms that the selected symbol period is greater than the multipath delay spread, as modeled in Section II.

Figures 5 and 6 depict receiver BER performance in the tank when the CFOs between the receiver and the two transmitters are set to $\Delta f_{1,1} = -\Delta f_{2,1} = 15$ Hz and the TOs are set to $\tau_{1,1} = \frac{100}{256}T_s$, $\tau_{2,1} = 0$ and $\tau_{1,1} = \frac{40}{256}T_s$, $\tau_{2,1} = 0$, respectively. We observe that under both scenaria, the proposed receiver exhibits superior performance. For example, in Fig. 5, when $\tau_{1,1} = \frac{100}{256}T_s$, $\tau_{2,1} = 0$, the proposed receiver achieves a BER of 10^{-4} for signal-to-noise ratio (SNR) between 18 to 20 dB, while the BER of the three other receiver designs that do not account for TOs and CFOs is around 0.4 for the same SNR. In addition, in Figures 5 and 6 we observe that when the receiver does not account for CFOs, it exhibits poor BER performance regardless of the SNR level. Furthermore, by comparing the BER performance results depicted in Figures 5 and 6, we observe that larger TOs (i.e. $\tau_{1,1} = \frac{100}{256}T_s$ and $\tau_{2,1} = 0$) have significantly more negative impact, when the receiver does not account for multiple TOs. However, the BER performance of the proposed receiver for large TOs is significantly better for higher SNRs.

Figures 7 and 8 illustrate the BER performance in the tank when the CFOs between the receiver and the two transmitters are set to $\Delta f_{1,1} = -\Delta f_{2,1} = 1.5$ Hz and the TOs are set to $\tau_{1,1} = \frac{100}{256}T_s$, $\tau_{2,1} = 0$ and $\tau_{1,1} = \frac{40}{256}T_s$, $\tau_{2,1} = 0$,

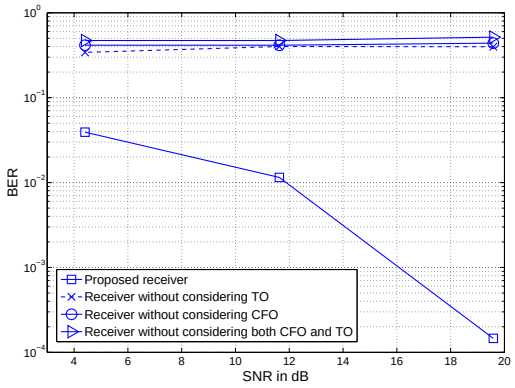

Fig. 5. Performance of the receiver design in tank when $\Delta f_{1,1} = -\Delta f_{2,1} = 15$ Hz, $\tau_{1,1} = \frac{100}{256}T_s$ and $\tau_{2,1} = 0$.

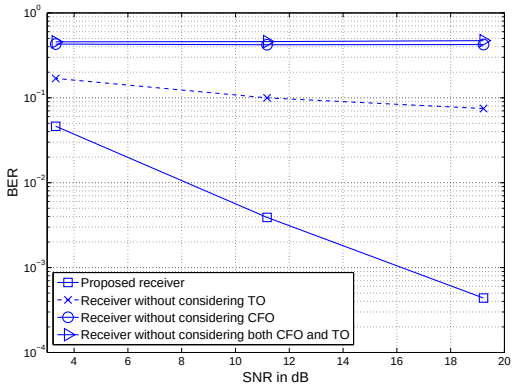

Fig. 6. Performance of the receiver design in tank when $\Delta f_{1,1} = -\Delta f_{2,1} = 15$ Hz, $\tau_{1,1} = \frac{40}{256}T_s$ and $\tau_{2,1} = 0$.

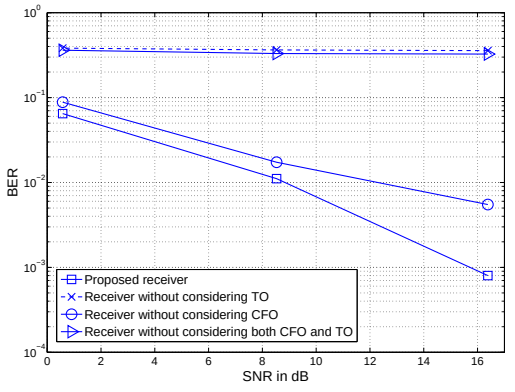

Fig. 7. Performance of the receiver design in tank when $\Delta f_{1,1} = -\Delta f_{2,1} = 1.5$ Hz, $\tau_{1,1} = \frac{100}{256}T_s$ and $\tau_{2,1} = 0$.

respectively. We observe that the proposed receiver exhibits superior performance in both cases. For instance, in Fig. 7, when $\tau_{1,1} = \frac{100}{256}T_s$, $\tau_{2,1} = 0$, the proposed receiver achieves a BER of 10^{-3} for SNR between 16 to 18 dB, while the BER of the receiver that does not account for CFOs is close to 10^{-2}. Receiver designs that either account for CFOs or do

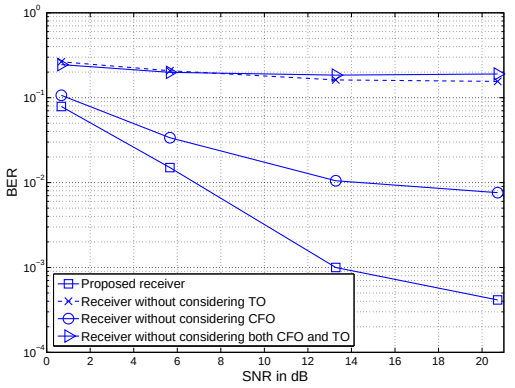

Fig. 8. Performance of the receiver design in tank when $\Delta f_{1,1} = -\Delta f_{2,1} = 1.5$ Hz, $\tau_{1,1} = \frac{40}{256}T_s$ and $\tau_{2,1} = 0$.

not account for both TOs and CFOs exhibit BER performance close to 0.3 regardless of the SNR level. Additionally, by comparing the BER performance results depicted in Fig. 7 and Fig. 5, we observe that larger CFOs have notably more negative impact on the BER performance, when the receiver does not account for multiple CFOs.

B. Lake Tests

A second software-defined underwater acoustic testbed of $M_t = 2$ distributed transmitters and $M_r = 1$ receiver is deployed near the small boat harbor in Buffalo Port of Lake Erie, as shown in Fig. 9. Distributed transmitters operate at the same power and carrier frequency, $f_c = 100$ kHz. The hardware specifications of the acoustic transducer TC4013 guarantee a flat frequency response in the selected region of frequencies for both tank and Lake experiments. The receiver is deployed 450 ft apart from the transmitters, while the two transmitters are positioned 15 ft apart from each other. All three transceivers are submerged in approximate depth of 25 ft. Fig. 10 illustrates the normalized channel response during Lake Erie experiments. We observe that multipath attenuates faster (as expected due to increased deployment distance and depth) when compared to the channel response observed in Fig. 4.

Figures 11 and 12 show receiver BER performance in Lake Erie when the CFOs between the receiver and the two transmitters are set to $\Delta f_{1,1} = -\Delta f_{2,1} = 15$ Hz and the TOs are set to $\tau_{1,1} = \frac{100}{256}T_s$, $\tau_{2,1} = 0$ and $\tau_{1,1} = \frac{40}{256}T_s$, $\tau_{2,1} = 0$, respectively. For $\tau_{1,1} = \frac{100}{256}T_s$ and $\tau_{2,1} = 0$, the proposed receiver achieves BER of 0 at SNR around 28 dB (not depicted) while the other three receivers perform poorly with BER close to 0.5. When $\tau_{1,1} = \frac{40}{256}T_s$ and $\tau_{2,1} = 0$, the proposed receiver achieves BER of 1.428×10^{-5} at SNR around 28 dB (not depicted) while the receiver that does not account for TOs achieves BER of 0.0047. BERs of the other two receiver designs are close to 0.4. We observe that in both Figures 11 and 12, the proposed receiver exhibits superior BER performance. For example, in Fig. 11, when $\tau_{1,1} = \frac{100}{256}T_s$, $\tau_{2,1} = 0$, the proposed receiver achieves a BER of 10^{-4} for SNR between 18 to 20 dB, while the BER of

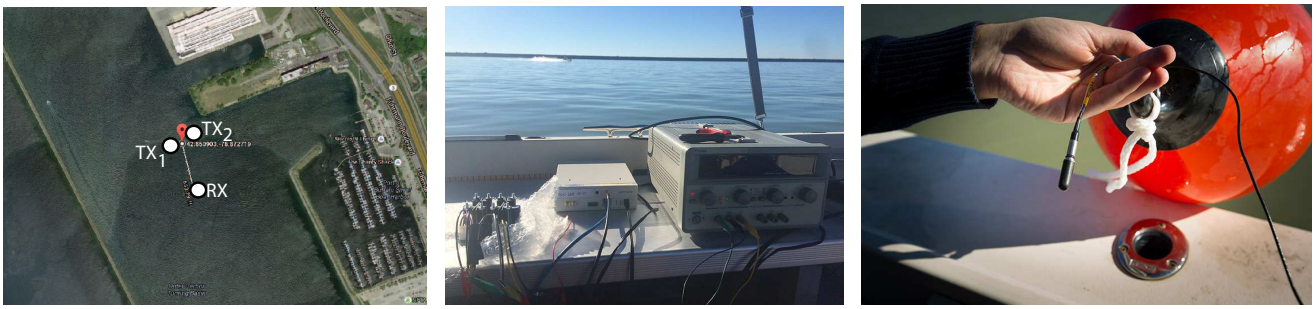

Fig. 9. Lake Erie testbed setup: Two software-defined acoustic transmit and one receive modems (center) are interfaced with $M_t = 2$ and $M_r = 1$ acoustic transducers (right), respectively, and are deployed in the small boat harbor at Buffalo Port (left).

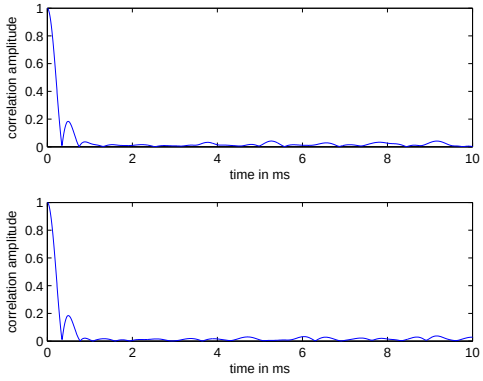

Fig. 10. Normalized channel response in Lake Erie.

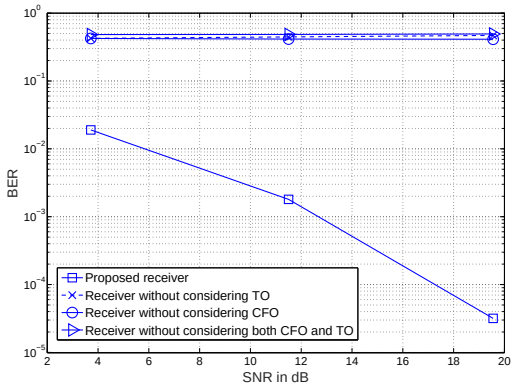

Fig. 11. Performance of the receiver design in lake when $\Delta f_{1,1} = -\Delta f_{2,1} = 15$ Hz, $\tau_{1,1} = \frac{100}{256}T_s$ and $\tau_{2,1} = 0$.

the other three receivers that do not account for TOs and CFOs is around 0.4 for the same SNR values. We observe that BER results acquired in Lake Erie are consistent to the BER performance results observed during tank tests. More specifically, based on the tank tests the receiver that does not account for multiple CFOs performs poorly at all SNR levels. In addition, larger TOs (i.e. $\tau_{1,1} = \frac{100}{256}T_s$ and $\tau_{2,1} = 0$) affect the BER performance of the proposed receiver less severely for higher SNRs.

Figures 13 and 14 illustrate the BER performance in Lake

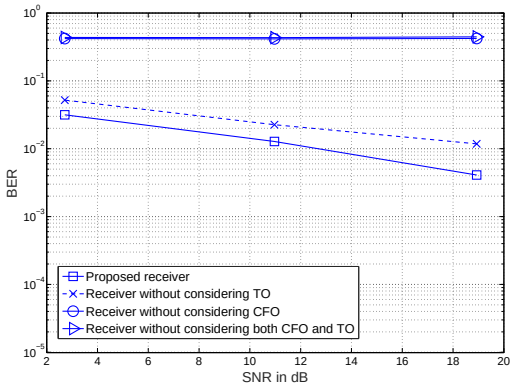

Fig. 12. Performance of the receiver design in lake when $\Delta f_{1,1} = -\Delta f_{2,1} = 15$ Hz, $\tau_{1,1} = \frac{40}{256}T_s$ and $\tau_{2,1} = 0$.

Erie when the CFOs between the receiver and the two transmitters are set to $\Delta f_{1,1} = -\Delta f_{2,1} = 1.5$ Hz and the TOs are set to $\tau_{1,1} = \frac{100}{256}T_s$, $\tau_{2,1} = 0$ and $\tau_{1,1} = \frac{40}{256}T_s$, $\tau_{2,1} = 0$, respectively. When $\tau_{1,1} = \frac{100}{256}T_s$ and $\tau_{2,1} = 0$, both the proposed receiver and receiver that does not account for CFOs achieve BER of 0 at SNR around 28 dB, while the other two receivers perform poorly with BER close to 0.5. When $\tau_{1,1} = \frac{40}{256}T_s$ and $\tau_{2,1} = 0$, the proposed receiver achieves BER of 0 at SNR around 28 dB (not depicted), while the receiver that does not account for multiple CFOs achieves BER of 2.016×10^{-4}. BERs of receiver designs that account for CFOs only and receivers that do not account for both CFOs and TOs are 0.0056 and 0.0112, respectively. We observe that the proposed receiver exhibits superior BER performance in both Figures 13 and 14. For instance, in Fig. 13, when $\tau_{1,1} = \frac{100}{256}T_s$, $\tau_{2,1} = 0$, the proposed receiver achieves 3 dB gain at a BER of 10^{-4} compared to the receiver that does not account for CFOs. Receiver designs that either account for CFOs only or do not account for both TOs and CFOs exhibit BER performance close to 0.3, regardless of the SNR level. Furthermore, by comparing the BER performance results depicted in Fig. 13 and Fig. 11, we observe that larger CFOs (i.e. $\Delta f_{1,1} = -\Delta f_{2,1} = 15$ Hz) have notably more negative impact on the BER performance, when the receiver does not account for CFOs. This result is also consistent to the

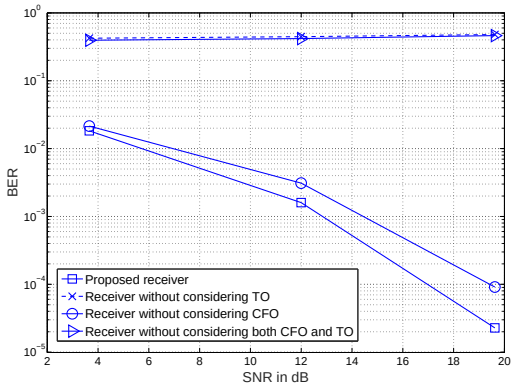

Fig. 13. Performance of the receiver design in lake when $\Delta f_{1,1} = -\Delta f_{2,1} = 1.5$ Hz, $\tau_{1,1} = \frac{100}{256}T_s$ and $\tau_{2,1} = 0$.

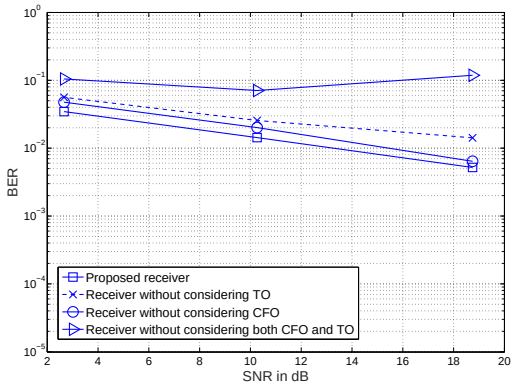

Fig. 14. Performance of the receiver design in lake when $\Delta f_{1,1} = -\Delta f_{2,1} = 1.5$ Hz, $\tau_{1,1} = \frac{40}{256}T_s$ and $\tau_{2,1} = 0$.

observations from the tank tests.

Both tank and Lake Erie experiments consider greater than $\lambda = c/f = 1.5$ cm (0.6 inches) transmit antenna deployments to ensure channel independence. However, in both cases transmit antennas' distance from the receiver is approximately the same, thus resulting in the same propagation delay between the two links. Therefore, the above selected time offsets (i.e. $\tau_{1,1} = \frac{40}{256}T_s$ and $\tau_{1,1} = \frac{100}{256}T_s$) correspond to transmission delays that are synthetically introduced to the SDAMs. The same process was followed for carrier frequency offsets, $\Delta f_{1,1} = 1.5$ Hz and $\Delta f_{1,1} = 15$ Hz. Both synthetically generated CFOs and TOs were accordingly estimated by the proposed receiver design. The selected CFOs reflect a range of typical frequency skew values (15-150 parts-per-million) for clock crystals, while they also correspond to low mobility speeds of 0.02 m/s and 0.2 m/s, respectively.

V. Conclusion

In this paper, we designed, implemented, and experimentally validated a receiver front-end design that is able to accommodate multiple CFOs and multiple TOs and account for symbol energy attenuation in distributed UWA MIMO systems. The proposed receiver was implemented in GNU Radio software. Two software-defined testbeds with in-house built SDAMs were also built to evaluate in real-time the BER performance of the proposed receiver design. Real-world testbed deployments were performed in both indoor (tank) and outdoor (lake) environments. Extensive experiments demonstrated that the proposed receiver addresses effectively the adverse effects of multiple CFOs and multiple TOs on the received signal energy and exhibits superior BER performance when compared to the current state-of-the-art. The proposed receiver design may be particularly suited for narrowband cooperative network localization, navigation and related applications in distributed underwater networks.

References

[1] T. Melodia, H. Kulhandjian, L. Kuo, and E. Demirors, "Advances in Underwater Acoustic Networking," in *Mobile Ad Hoc Networking: Cutting Edge Directions*, second edition ed., S. Basagni, M. Conti, S. Giordano, and I. Stojmenovic, Eds. Inc., Hoboken, NJ: John Wiley and Sons, 2013, pp. 804–852.

[2] L. Liu, S. Zhou, and J. Cui, "Prospects and problems of wireless communication for underwater sensor networks," *Wirel. Commun. Mob. Comput.*, vol. 8, no. 8, pp. 977–994, Oct. 2008. [Online]. Available: http://dx.doi.org/10.1002/wcm.v8:8

[3] M. A. Alvarez, B. Azari, and U. Spagnolini, "Time and frequency self-synchronization in dense cooperative network," in *2014 48th Asilomar Conference on Signals, Systems and Computers*, Nov 2014, pp. 1811–1815.

[4] F. Wang and M. Ingram, "A practical equalizer for cooperative delay diversity with multiple carrier frequency offsets," in *Communications (ICC), 2012 IEEE International Conference on*, Jun 2012, pp. 4100–4104.

[5] H. Wang, Q. Y. X. Xia, and L. Bai, "A distributed linear convolutive space-frequency coding for cooperative communication systems with multiple frequency offsets," in *Communications. ICC. IEEE Int., Dresden*, 2009, pp. 1–5.

[6] W. Kuo and M. P. Fitz, "Frequency offset compensation of pilot symbol assisted modulation in frequency flat fading," *IEEE Transactions on Communications*, vol. 45, no. 11, pp. 1412–1416, Nov 1997.

[7] K. Tu, T. M. Duman, J. G. Proakis, and M. Stojanovic, "Cooperative mimo-ofdm communications: Receiver design for doppler-distorted underwater acoustic channels," in *2010 Conference Record of the Forty Fourth Asilomar Conference on Signals, Systems and Computers*, Nov 2010, pp. 1335–1339.

[8] J. Huang, S. Zhou, and Z. Wang, "Performance results of two iterative receivers for distributed mimo ofdm with large doppler deviations," *IEEE Journal of Oceanic Engineering*, vol. 38, no. 2, pp. 347–357, April 2013.

[9] Y. Cao, W. Su, and S. N. Batalama, "Distributed MIMO systems: Receiver design and ML detection," in *2016 IEEE International Conference on Acoustics, Speech and Signal Processing (ICASSP)*, March 2016, pp. 3566–3570.

[10] G. Sklivanitis, E. Demirors, S. N. Batalama, T. Melodia, and D. A. Pados, "Receiver configuration and testbed development for underwater cognitive channelization," in *2014 48th Asilomar Conference on Signals, Systems and Computers*, Nov 2014, pp. 1594–1598.

[11] E. Demirors, G. Sklivanitis, G. E. Santagati, T. Melodia, and S. N. Batalama, "Design of a software-defined underwater acoustic modem with real-time physical layer adaptation capabilities," in *Proceedings of the International Conference on Underwater Networks & Systems*, ser. WUWNET '14. New York, NY, USA: ACM, 2014, pp. 25:1–25:8. [Online]. Available: http://doi.acm.org/10.1145/2671490.2674473

[12] E. Demirors, G. Sklivanitis, T. Melodia, S. N. Batalama, and D. A. Pados, "Software-defined underwater acoustic networks: toward a high-rate real-time reconfigurable modem," *IEEE Communications Magazine*, vol. 53, no. 11, pp. 64–71, November 2015.

[13] P. Qarabaqi and M. Stojanovic, "Statistical modeling of a shallow water acoustic communication channel," in *Underwater Acoustic Measurements Conference*, Jun 2009, pp. 1341–1350.

[14] M. Stojanovic, "Underwater acoustic communications: Design considerations on the physical layer," in *IEEE/IFIP Fifth Annual Conference on Wireless on Demand Network Systems and Services (WONS 2008)*, Garmisch-Partenkirchen, Germany, Jan 2008.